Homogenized Crack Model for Finite Element Analysis of Concrete Fracture

H.-W. Song, C.-S. Bang, J.-W. Nam & K.-J. Byun
School of Civil & Environmental Engineering, Yonsei University, Seoul, Korea

ABSTRACT: Since quasi-brittle materials like concrete show strain localization behavior accompanied by strain softening, a numerical drawback such as mesh sensitivity is appeared in the finite element analysis. In this study, the so-called homogenized crack model is introduced for three dimensional finite element analysis of fracture in concrete both under tension and under multi-axial compression. A homogenization technique for a homogenized crack element having a velocity discontinuity is employed to remove the mesh sensitivity in finite element analysis of concrete fracture. A conventional elasto-plastic algorithm with an exponential softening rule in which the thickness of the crack is implicitly retained is applied for the constitutive model of tensile fracture and a Drucker-Prager type model with an exponential type of softening parameter is also applied for the constitutive model for compressive fracture of concrete under low confining pressure. Numerical examples show that softening behavior of concrete fracture is successfully predicted without mesh sensitivity using the homogenized crack model.

Keywords: Homogenized Crack Model, Strain Localization, Fracture Behavior of Concrete, Finite Element Analysis

1 INTRODUCTION

Concrete normally contains early-age micro-cracks due to thermal expansion and restrained shrinkage. Under certain loading condition, these micro-cracks may localize to a major macro crack and may result in failure of concrete. The softening behavior of concrete can be characterized as load resistant capacity after peak and localized strain. A numerical application of the strain softening makes loss of ellipticity of governing equation and boundary value problem becomes ill-posed. Consequently, a numerical drawback such as mesh sensitivity is appeared in the finite element analysis. Recently, various models have been proposed to solve these problems. As a model for progressive fracture analysis of concrete using finite element method, the so-called embedded crack model that introduces the internal discontinuity surface in an element is introduced by Wan et al. (1990). In strain localization problem, Oliver (2000) proposed discontinuity model that presumes fracture of concrete as phenomenon of discontinuity.

Multi-axial compressive fracture of concrete shows more complicated behavior than tensional failure behavior due to confining effect. In case of biaxial and triaxial compressive loading condition, the failure behavior of concrete is different from that of uniaxial and it shows more complex behavior (van Mier, 1984). Generally, it is known that the compressive failure behavior can be characterized by inclined shear-band crack fracture under uniaxial, biaxial and triaxial compression.

In this study, the so-called homogenized crack model is proposed for the finite element analysis of concrete fracture. Three-dimensional finite element analysis program has been developed for the analysis using the models which adopt softening type constitutive laws. Numerical results show that the mesh sensitivity problem can be overcome by using the model, and concrete fracture behavior under various load condition can be simulated comparably well with developed program.

2 FAILURE BEHAVIORS OF CONCRETE

2.1 *Uniaxial Compressive Strain Softening Behavior*

Based on experimental observations for uniaxial compressive concrete fracture, the softening stress-strain relationship may be depicted as in Figure 1.

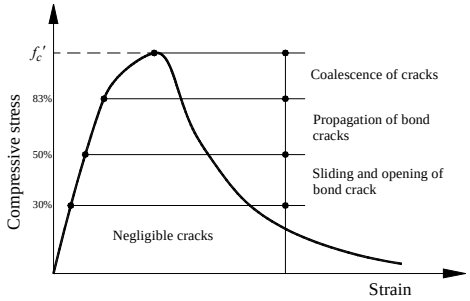

Figure 1. Stress-strain relationship under uniaxial compression.

In the post peak regime, strain distribution is not continuous and it is not easy to capture strain distribution exactly for the analysis of concrete fracture. Generally, the softening part of stress-strain curve shows structural properties due to the dependency of size of specimens rather than material property. From the results of compression test for the specimens of different heights (van Mier, 1984), the softening part of stress-strain curve shows size effect (Fig. 2a). But, the stress-displacement curve shows unique softening curve regardless of the specimen size (Fig. 2b).

2.2 *Biaxial Failure Behavior*

The failure behavior of concrete under confined stresses shows different behavior from that under uniaxial compressive behavior. Fig. 3a shows a typical stress-strain relationship for concrete subjected to biaxial loading (Kupfer et al. 1969). Due to confining effect, axial and lateral strains at maximum or ultimate point increase with the increment of confining pressure and concrete under compressive loading with confining pressure shows more ductile behavior before crushing.

Fig. 3b shows the volume dilatation behavior. When unstable crack propagation begins, volumetric strain increases due to considerable growth of micro cracks in mortar.

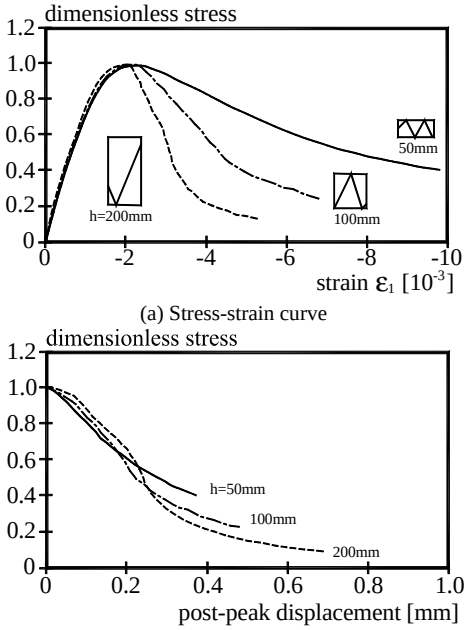

(a) Stress-strain curve

(b) Stress-displacement curve

Figure 2. Influence of slenderness of concrete specimens (van Mier, 1984).

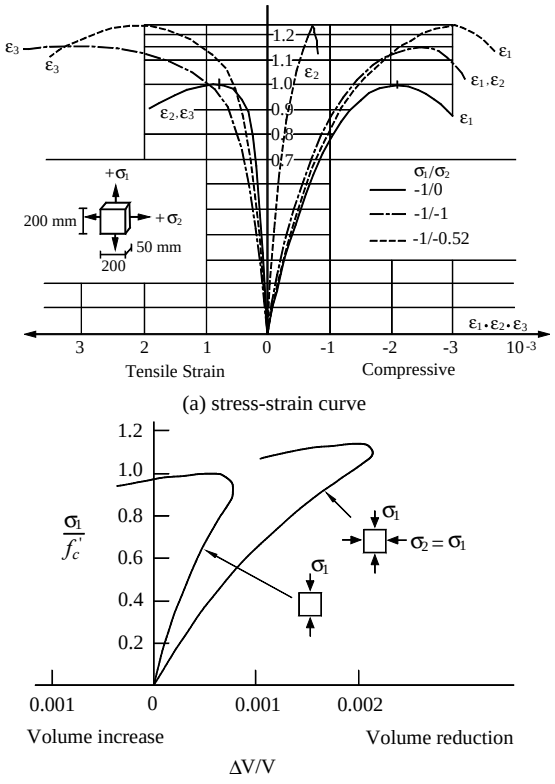

(a) stress-strain curve

(b) stress versus volumetric strain

Figure 3. Stress-strain response for concrete subjected to biaxial loading (Kupfer et al. 1969).

2.3 *Tensile Localized Failure Behavior*

Stress-strain curve of concrete under uniaxial tensile loading shows similar softening behavior as for the compressive stress-strain relationship. Strain localization also occurs for tensile behavior.

Softening (B region in Fig. 4) is shown in the localization region and unloading is shown at the other regions (A region in Fig. 4). The stress versus crack opening displacement relationship can be more adequate to represent the characteristics of concrete under tension than the stress versus strain relationship.

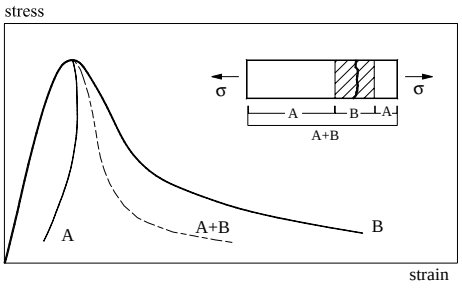

Figure 4. stress versus strain relationship under uniaxial tensile load.

3 HOMOGENIZED CRACK MODEL AND ANALYTICAL IMPLEMENTATION

3.1 *Homogenized Crack Model*

In this section, the so-called homogenized crack model is discussed in the frame of three-dimensional finite element formulation. A regularization technique for a continuum having velocity discontinuity is applied as a crack smeared into concrete.

Stress rate and strain rate of concrete and of crack within a representative elementary volume (REV) (Fig. 5) are denoted by $\dot{\boldsymbol{\sigma}}^i$, $\dot{\boldsymbol{\varepsilon}}^i$ and $\dot{\boldsymbol{\sigma}}^j$, $\dot{\boldsymbol{\varepsilon}}^j$, respectively, and following mixture rule can be established:

$$\dot{\boldsymbol{\sigma}} = \mu_i \dot{\boldsymbol{\sigma}}^i + \mu_j \dot{\boldsymbol{\sigma}}^j, \dot{\boldsymbol{\varepsilon}} = \mu_i \dot{\boldsymbol{\varepsilon}}^i + \mu_j \dot{\boldsymbol{\varepsilon}}^j \tag{1}$$

where, μ_i and μ_j are the volume fraction of concrete and crack, which satisfy Equation (2). The thickness of the crack in the REV is denoted by t in Fig. 5.

$$\mu_i + \mu_j = 1 \tag{2}$$

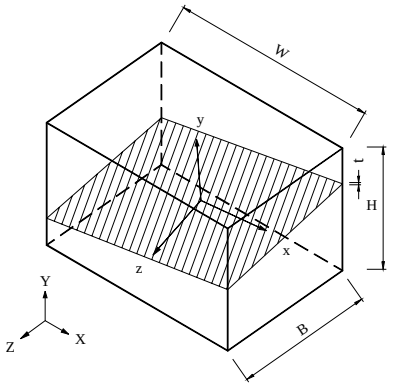

Figure 5. Representative elementary volume.

The equilibrium equations as well as compatibility conditions in the interface between concrete and crack surface can be established by assuming that the crack has finite material properties such as normal and shear stiffnesses. In local coordinate system, these equations are as follows:

$$\dot{\sigma}_{yy} = \dot{\sigma}^i_{yy} = \dot{\sigma}^j_{yy}, \dot{\tau}_{xy} = \dot{\tau}^i_{xy} = \dot{\tau}^j_{xy}, \dot{\tau}_{yz} = \dot{\tau}^i_{yz} = \dot{\tau}^j_{yz} \tag{3}$$

$$\dot{\varepsilon}_{xx} = \dot{\varepsilon}^i_{xx} = \dot{\varepsilon}^j_{xx}, \dot{\varepsilon}_{zz} = \dot{\varepsilon}^i_{zz} = \dot{\varepsilon}^j_{zz}, \dot{\gamma}_{zx} = \dot{\gamma}^i_{zx} = \dot{\gamma}^j_{zx} \tag{4}$$

It is noted that these relationships are similar to those introduced in the modified Voigt-Reuss model (Yamaguchi & Chen, 1990). The thickness of a crack inside concrete is negligibly small compared to the size of the finite element and the following velocity discontinuities in the normal and shear direction of the crack can be introduced:

$$\dot{\boldsymbol{g}} = \{\dot{g}_y, \dot{g}_x, \dot{g}_z\}^{\mathrm{T}} \tag{5}$$

Then, a constitutive equation for the crack is denoted by:

$$[\delta]\dot{\boldsymbol{\sigma}}^j = [K]\dot{\boldsymbol{g}} \tag{6}$$

where, $[\delta]$ is a 3×6 matrix and $[K]$ is the crack stiffness matrix defined as follows:

$$[\delta] = \begin{bmatrix} 0 & 1 & 0 & 0 & 0 & 0 \\ 0 & 0 & 0 & 1 & 0 & 0 \\ 0 & 0 & 0 & 0 & 1 & 0 \end{bmatrix} [K] = \begin{bmatrix} K_{11} & K_{12} & K_{13} \\ K_{21} & K_{22} & K_{23} \\ K_{31} & K_{32} & K_{33} \end{bmatrix} \tag{7}$$

Meanwhile, constitutive equation of the concrete can be modeled with a constitutive matrix $[D]$ as:

$$\dot{\boldsymbol{\sigma}}^i = [D]\dot{\boldsymbol{\varepsilon}}^i \tag{8}$$

By assuming the crack thickness $t \ll$ H and $\dot{\boldsymbol{g}} := t[\delta]\dot{\boldsymbol{\varepsilon}}^j$, Equation 1b becomes

$$[\delta]\dot{\boldsymbol{\varepsilon}} \approx [\delta]\dot{\boldsymbol{\varepsilon}}^i + \mu\dot{\boldsymbol{g}} \tag{9}$$

where, μ=t/H in Figure 5. It should be noted that this assumption is different from the formulation of strong discontinuity (Wells & Sluys, 2001), where the width of the localization band tends to zero. In this case, the homogenization technique with two different components is introduced. Equations 3, 6 and 8 can be rearranged as follows for an equation for the strain rate of concrete:

$$[\delta]\dot{\boldsymbol{\varepsilon}}^{i} = [A]\dot{\boldsymbol{\varepsilon}} + [B]\dot{\boldsymbol{g}} \tag{10}$$

where,

$$[A]=\begin{bmatrix} -\frac{D_{21}}{C_1} & -\frac{K_{11}}{\mu C_1} & -\frac{D_{23}}{C_1} & -\frac{D_{24}}{C_1} & -\frac{D_{25}}{C_1} & -\frac{D_{26}}{C_1} \\ -\frac{D_{41}}{C_2} & -\frac{D_{42}}{C_2} & -\frac{D_{43}}{C_2} & -\frac{K_{22}}{\mu C_2} & -\frac{D_{45}}{C_2} & -\frac{D_{46}}{C_2} \\ -\frac{D_{51}}{C_3} & -\frac{D_{52}}{C_3} & -\frac{D_{53}}{C_3} & -\frac{D_{54}}{C_3} & -\frac{K_{33}}{\mu C_3} & -\frac{D_{56}}{C_3} \end{bmatrix} \tag{11}$$

and,

$$[B]=\begin{bmatrix} 0 & \frac{K_{12}+\mu D_{24}}{C_1} & \frac{K_{13}+\mu D_{25}}{C_1} \\ \frac{K_{21}+\mu D_{42}}{C_2} & 0 & \frac{K_{23}+\mu D_{45}}{C_2} \\ \frac{K_{31}+\mu D_{52}}{C_3} & \frac{K_{32}+\mu D_{54}}{C_3} & 0 \end{bmatrix} \tag{12}$$

with

$$C_1 = D_{22} + \frac{K_{11}}{\mu}, C_2 = D_{44} + \frac{K_{22}}{\mu}, C_3 = D_{55} + \frac{K_{33}}{\mu} \tag{13}$$

Using Equations 9 and 10, we obtain

$$[\delta]\dot{\boldsymbol{\varepsilon}}^{i} = [S]\dot{\boldsymbol{\varepsilon}} \tag{14}$$

where

$$[S] = ([I] + \frac{1}{\mu}[B])^{-1}([A] + \frac{1}{\mu}[B][\delta]) \tag{15}$$

or

$$\dot{\boldsymbol{\varepsilon}}^{i} = [S_1]\dot{\boldsymbol{\varepsilon}} \tag{16}$$

where

$$[S_1]=\begin{bmatrix} 1 & 0 & 0 & 0 & 0 & 0 \\ S_{11} & S_{12} & S_{13} & S_{14} & S_{15} & S_{16} \\ 0 & 0 & 1 & 0 & 0 & 0 \\ S_{21} & S_{22} & S_{23} & S_{24} & S_{25} & S_{26} \\ S_{31} & S_{32} & S_{33} & S_{34} & S_{35} & S_{36} \\ 0 & 0 & 0 & 0 & 0 & 1 \end{bmatrix} \tag{17}$$

Thus, constitutive equation for the crack can be obtained from Equations 9 and 16, i.e.

$$\dot{\boldsymbol{g}} = [S_2]\dot{\boldsymbol{\varepsilon}} \tag{18}$$

where,

$$[S_2] = \frac{1}{\mu}([\delta] - [S]) \tag{19}$$

Finally, an averaged constitutive equation of the concrete having a crack inside can be derived from Equations 1, 8 and 16 as,

$$\dot{\boldsymbol{\sigma}} = [D^{eq}]\dot{\boldsymbol{\varepsilon}},\ [D^{eq}] = [D][S_1] \tag{20}$$

3.2 *Initiation and Propagation of Crack*

Assuming that crack occurs when determinant of acoustic tensor becomes zero initiation and propagation of crack be satisfied the bifurcation condition as below:

$$F(\boldsymbol{n}) = \det(n_i\, D^{eq}_{ijkl}\, n_l) = 0 \tag{21}$$

Where, directional vectors ***n*** and ***m***, expressed as fourth order polynomial equation in two-dimension, determine the shape of localization. In case of three-dimension, the solution can be determined using the Lagrangian equation (Leroy & Ortiz, 1989). In order to determine initiation and direction of crack in concrete using Equation 21, a calculation using spherical coordination as shown in Figure 6 is used with Equation 22 as,

$$n = (\cos\phi\cos\theta, \cos\phi\sin\theta, \sin\theta)\ ,$$

$$0 < \phi < \frac{1}{2\pi},\ 0 < \theta < 2\pi \tag{22}$$

First approximated minimum value can be determined through iterative calculations per each incremental angle.

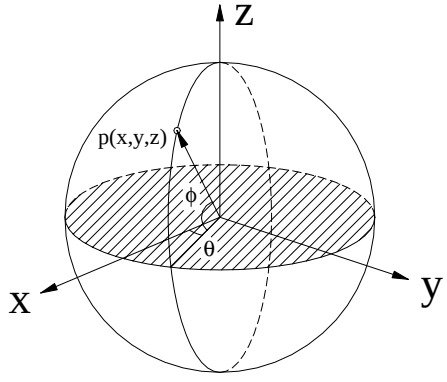

Figure 6. Spherical coordination.

For compressive failure analysis of concrete, yield criterion for compressive softening behavior is represented with two parameters, α and κ, in the Drucker-Prager model (Fig. 7) as below:

$$F = \alpha I_1 + \sqrt{J_2} - \kappa(\bar{\sigma}, \bar{\varepsilon}^p) = 0 \tag{23}$$

where I_1 and J_2 represents first invariant of stress and second invariant of deviatoric stress, respectively, and α is a constant and the $\kappa(\bar{\sigma}, \bar{\varepsilon}^p)$ expressed by effective stress, $\bar{\sigma}$ and effective plastic strain, $\bar{\varepsilon}^p$.

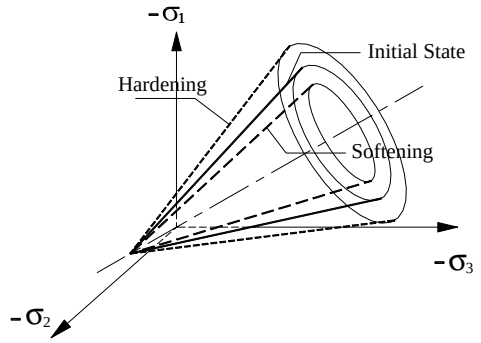

Figure 7. Failure criteria of Drucker-Prager.

In this study, a exponential type softening rule for isotropic softening is used as in Equation 24:

$$\kappa(\bar{\sigma}, \bar{\varepsilon}^p) = \kappa_0 \, e^{(\beta \bar{\sigma} \ \bar{\varepsilon}^p)^{2r}} \tag{24}$$

where κ_0 is initial softening constant, β and γ are the constants of material properties.

For the case of tensile fracture, a crack occurs perpendicular to the direction of principal stress when principal stress σ_1 exceeds tensile strength f_t, another softening rule as in Equation 25 is used:

$$F = \sigma_1 - f_t \, (e^{-\kappa(\eta \dot{g}_y^p)^{\lambda}}) \tag{25}$$

where κ, η and λ are material properties and $\dot{g}_y^p$ the amount of accumulated velocity discontinuity at crack surface. Once crack occurrence is perceived, the constitutive equation (Equation 20) is introduced at the element level. During this process, the crack stiffness in Equation 7 is updated according to the evolution law without considering interaction between normal stiffness and shear stiffness of crack surface, i.e.;

$$[\boldsymbol{K}] = \begin{bmatrix} K_N^{ep} & 0 & 0 \\ 0 & K_{S1}^{ep} & 0 \\ 0 & 0 & K_{S2}^{ep} \end{bmatrix} \tag{26}$$

where, K_N^{ep} is modified normal stiffness and K_{s1}^{ep} and K_{s2}^{ep} are modified shear stiffness. Once the crack is perceived at Gauss points of element level, the proposed homogenized crack element is substituted and the elastic prediction and plastic correction algorithm is introduced for the integration of the constitutive equation. Three dimensional solid elements with 20 nodal points are used for finite element discretization.

4 NUMERICAL ANALYSIS

4.1 *Uniaxial Compressive Failure*

For the verification of proposed model, a numerical analysis is carried out and compared with the experimental data (van Mier et al. 1997). A 10×10×20cm rectangular concrete specimen is discretized with 875 nodes and 144 elements as in Figure 8.

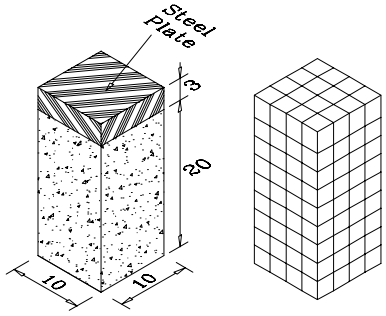

Figure 8. Modeling of concrete specimen.

The bifurcation analysis result shows that the direction of crack surface inclines about 27 degrees to the direction of compressive stress, which shows that shear failure occurs in concrete, as shown in Figure 9.

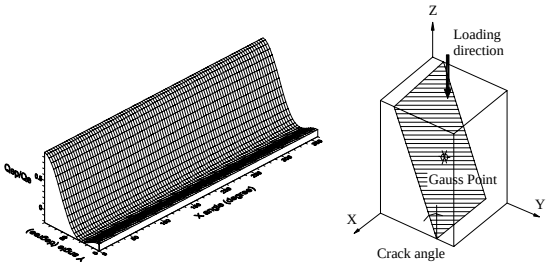

Figure 9. Determination of crack surface direction.

The result also shows that compressive strength and softening behavior is comparably well simulated with experimental result (Fig. 10). In the analysis, compressive strength of normal concrete, 210kgf/cm^2, is used and normal stiffness and shear

stiffness of crack surface, 260,000kg/cm^2/cm and 93,000kg/cm^2/cm are used, respectively. Localized deformation during the fracture of the concrete specimen is captured as shown in Figure 11. The mesh objectivity using the proposed model for different mesh designs is obtained as Figure 12. Since the stiffness of crack surface and velocity discontinuity in the homogenized crack model proposed in this study play a role as a characteristic length, the mesh sensitivity problem can be solved.

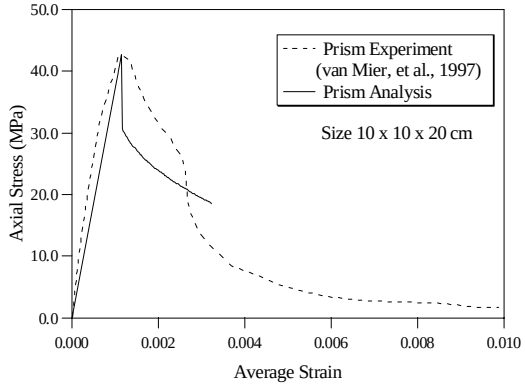

Figure 10. Stress-strain curve.

Figure 11. Shape of localized deformation during fracture.

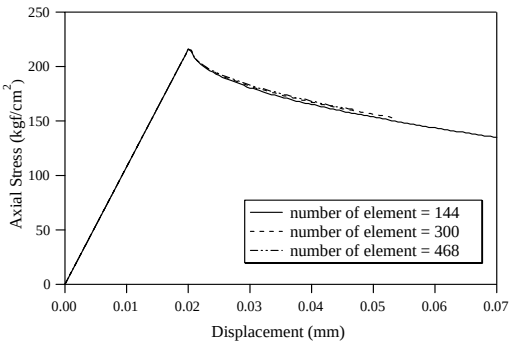

Figure 12. Stress-displacement curve according to different mesh designs.

4.2 *Multi-axial compressive failure*

Multi-axial compressive failure analysis is also carried out for concrete specimen subjected to different confinement as shown in Figure 13. The proposed model can simulated softening behavior during the failure.

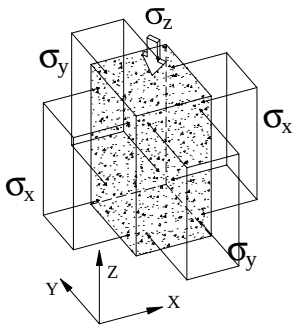

Figure 13. Multi-axial loading conditions.

Figure 14 shows the result of numerical analysis illustrated on the biaxial principal plane along with the experimental result of Kupfer et al. (1969) for comparison. The comparison shows that homogenized crack model can simulate the confinement effect. However, there is a little discrepancy between analytical result and experimental result due to different specimen sizes used in analysis and experiment, and no applied hardening rule in the analysis.

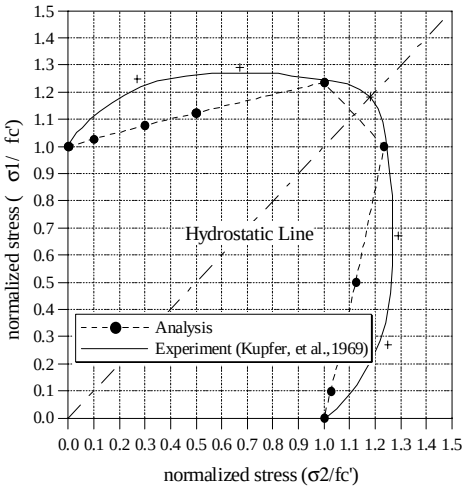

Figure 14. Normalized biaxial stress.

Strain variations in each direction and volumetric strain under different biaxial confining pressures are illustrated in Figure 15 and Figure 16, respectively. Figure 15 shows the confining effect

of concrete under biaxial compression and Figure 16 shows that the volume change decreases with the increase of confining pressure and it increases after peak strength.

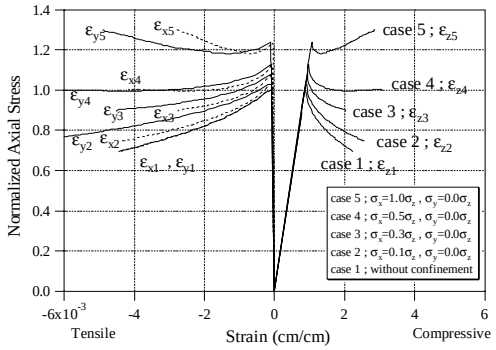

Figure 15. Normalized axial stress vs Strain.

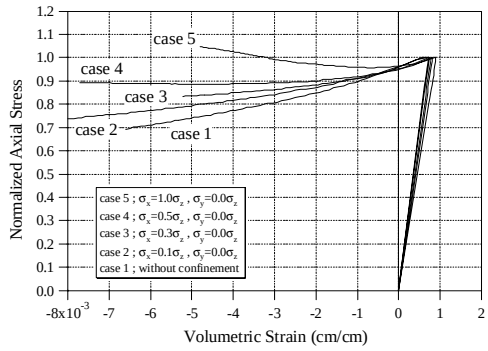

Figure 16. Volume strain relationship.

For the case of triaxial stresses, the increase of compressive strength due to the confinement can be simulated as shown in Figure 17. It is shown that more confinement effecet for triaxial state is obtained than for the biaxial stresses.

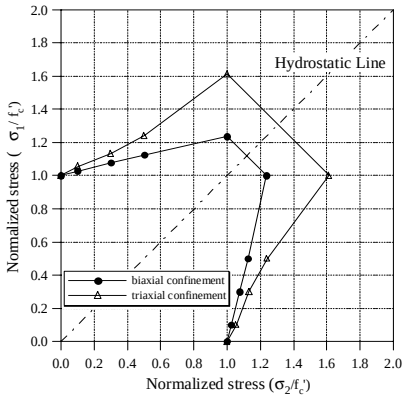

Figure 17. Tri-axial stress state.

4.3 *Uniaxial Tensile Failure*

Tensile failure analysis using the homogenized crack model is carried out for a plain concrete specimen with double notches (Figure 18) and the result is compared with an experimental data (Gopalaratnam & Shah 1985).

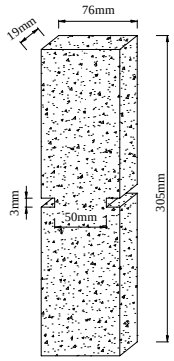

Figure 18. Model specimen with double notches.

As shown in Figure 19, the axial stress-axial deformation shows softening behavior with a small discrepancy in peak strength.

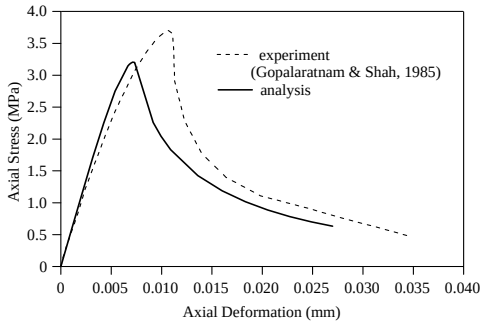

Figure 19. Axial stress-displacement relationship.

The mesh objectivity obtained using the proposed model is shown in Figure 20.

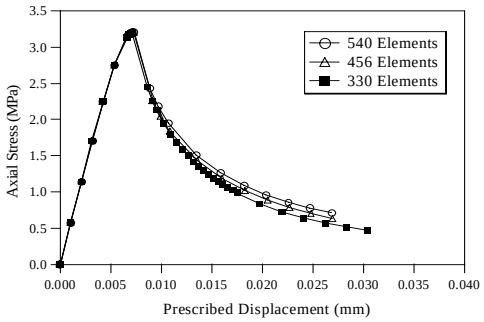

Figure 20. Stress-displacement relationship for different mesh designs.

5 CONCLUSIONS

Since concrete show strain localization behavior accompanied by strain softening, a pathological phenomenon such as mesh sensitivity is appeared in the numerical analysis. In this study, the so-called homogenized crack model, which considers velocity discontinuity in a constitutive equation, is proposed for a cracking and its propagation in strain softening regime of concrete. A constitutive equation for the proposed crack model is derived in the general three-dimensional space and finite element analysis is carried out for fracture analysis of concrete subjected to various loading conditions. Results from the numerical analysis are compared with experimental data. The comparison shows that the mesh sensitivity in the analysis is successfully overcome and failure behaviors of concrete are well simulated.

REFERENCES

Gopalaratnam, V.G. & Shah, S.P. 1985. Softeing response of plain concrete in direct tension. *ACI J.* 82: 310-323

Kupfer, H., Hilsdorf, H.K. & Rusch, H. 1969. Behavior of concrete under biaxial stresses. *J. of American Concrete Institute.* 66(8): 656-666

Leroy, Y. & Ortiz, M. 1989. Finite element analysis of strain localization in frictional materials. *Int. J. Numer. Anal. Mech. Geomech.* 13: 53-74

Oliver, J. 2000. On the discrete constitutive models induced by strong discontinuity; kinematics and continuum constitutive equations. *Int. J. of Solids & Structures.* 37: 7202-7229

van Mier, J.G.M. 1984. *Strain softening of concrete under multiaxial compression*. Ph.D. thesis, Eindhoven Univ. of Tech. Netherlands.

van Mier, J.G.M., et al. 1997. Strain-softening of concrete in uniaxial compression. *Materials & Structures. RILEM*. 30: 195-209

Wan, R.G., Chan, D.H. & Morgenstern, N.R. 1990. A finite element method for the analysis of shear bands in geomaterials. *Finite Elements in Analysis and Design.* 7: 129-143

Wells, G. N. & Sluys, L. J. 2001. A new method for modeling cohesive cracks using finite elements. *Int. J. Numer. Meth. Engng.* 50: 2667-2682

Yamaguchi, E. & Chen, W.F. 1990. Cracking model for finite element analysis of concrete materials. *J. of Engineering Mechanics. ASCE.* 116: 1242-1260